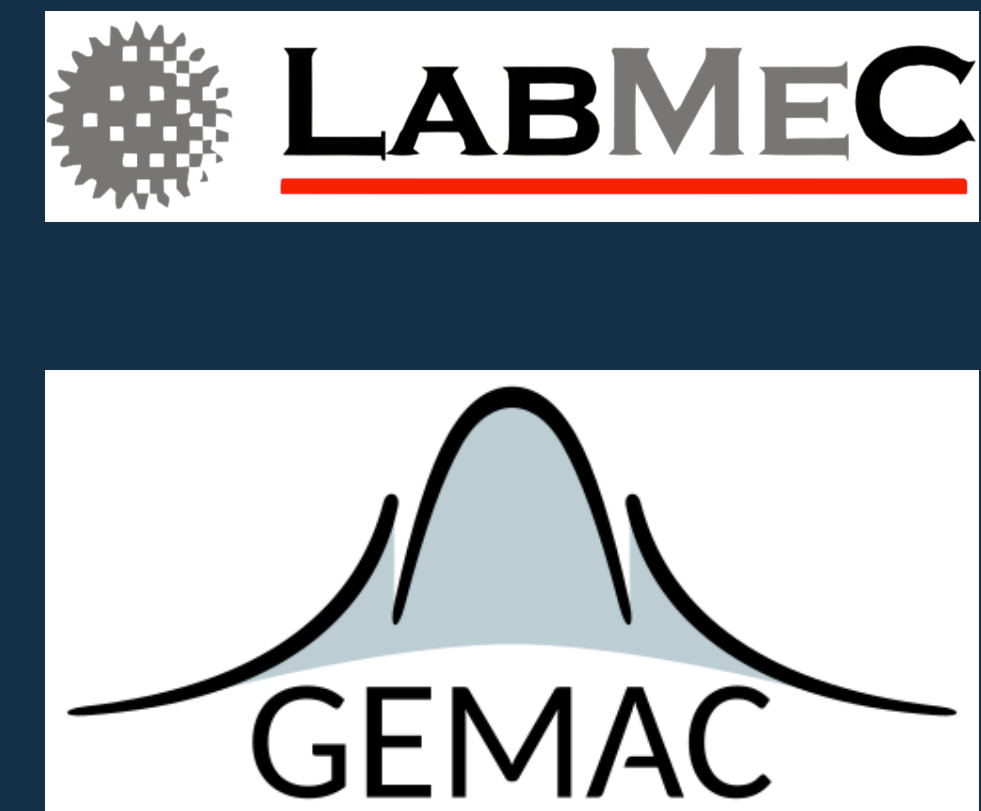


DEVELOPMENT OF HIGH-ORDER $H(\text{curl}, \Omega)$ -CONFORMING APPROXIMATION SPACES FOR PHOTONIC WAVEGUIDE ANALYSIS

Francisco T. Orlandini¹, Hugo E. H. Figueira¹ and Philippe R. B. Devloo²

¹School of Electrical and Computer Engineering, State University of Campinas, Brazil

²School of Civil Engineering, Architecture and Urban Design, State University of Campinas, Brazil



1. MOTIVATION

High precision approximation of dispersion parameters is a major concern in the design of photonic waveguides and the Computational Electromagnetics (CE) community has sought many different numerical techniques in order to achieve this requirement. In the present work, a high-order Finite Element Method (FEM) scheme is introduced, presenting high convergence rates and being able to deal with waveguides with curved cross-section and lossy inhomogeneous media with transverse anisotropy. The $H(\text{curl}; \Omega)$ -conforming elements used in the scheme are a hierarchical construction of the Nédélec elements of the first kind, implemented in the NeoPZ framework. The importance of using non-linear mapped elements when using high-order elements is discussed and real-world scenario results are presented. Finally, the hierarchical construction of the elements is explored in an example of how hp-adaptive finite elements can significantly reduce the number of equations while still achieving high precision results.

2. FEM FORMULATION AND THE $H(\text{curl}, \Omega)$ -CONFORMING ELEMENTS

The formulation used in this work performs modal analysis on the cross-section Ω of a waveguide for a given angular frequency ω , using $H(\text{curl}; \Omega)$ and $H^1(\Omega)$ -conforming elements for the transverse and longitudinal components of the electric field, respectively. It is valid for a domain composed of materials presenting at most transverse-anisotropy. From Jin [1]: Find non-trivial $(\beta^2, e_t, e_z) \in (\mathbb{C} \times [\mathbb{C}]^N \times [\mathbb{C}]^M)$ such that:

$$\int_{\Omega} \left\{ \sum_j^N e_{tj} [\mu_{zz}^{-1} (\nabla_t \times \varphi_j) \cdot (\nabla_t \times \varphi_i)^* - k_0^2 \epsilon_{xy} \varphi_j \cdot \varphi_i^*] + \beta^2 \sum_l^M e_{zk} \left[\sum_j^N e_{tj} \mu_{xy}^{-1} (\nabla_t \varphi_k + \varphi_j) \cdot (\nabla_t \varphi_k + \varphi_i)^* - k_0^2 \epsilon_{zz} \varphi_k \varphi_k^* \right] \right\} d\Omega = 0, \quad (1)$$

$\forall \varphi_i \in B_{U_h}, \varphi_k \in B_{V_h},$

where B_{U_h} and B_{V_h} denote the FEM basis for the finite-dimensional subspaces of $H(\text{curl}; \Omega)$ and $H^1(\Omega)$, respectively.

The $H(\text{curl}; \Omega)$ -conforming elements used in this work are the Nédélec elements of the first kind[2] and were constructed in the NeoPZ framework in a hierarchical manner.

3. EFFECTS OF GEOMETRICAL REPRESENTATION ON CONVERGENCE

In order to benefit from the high-order elements, non-linear mapped elements are essential when dealing with curved geometries. Figure 1 compares the convergence rate of the effective index n_{eff} for a step-index optical fiber with polynomial order $k = 4$, using three different types of mapped elements.

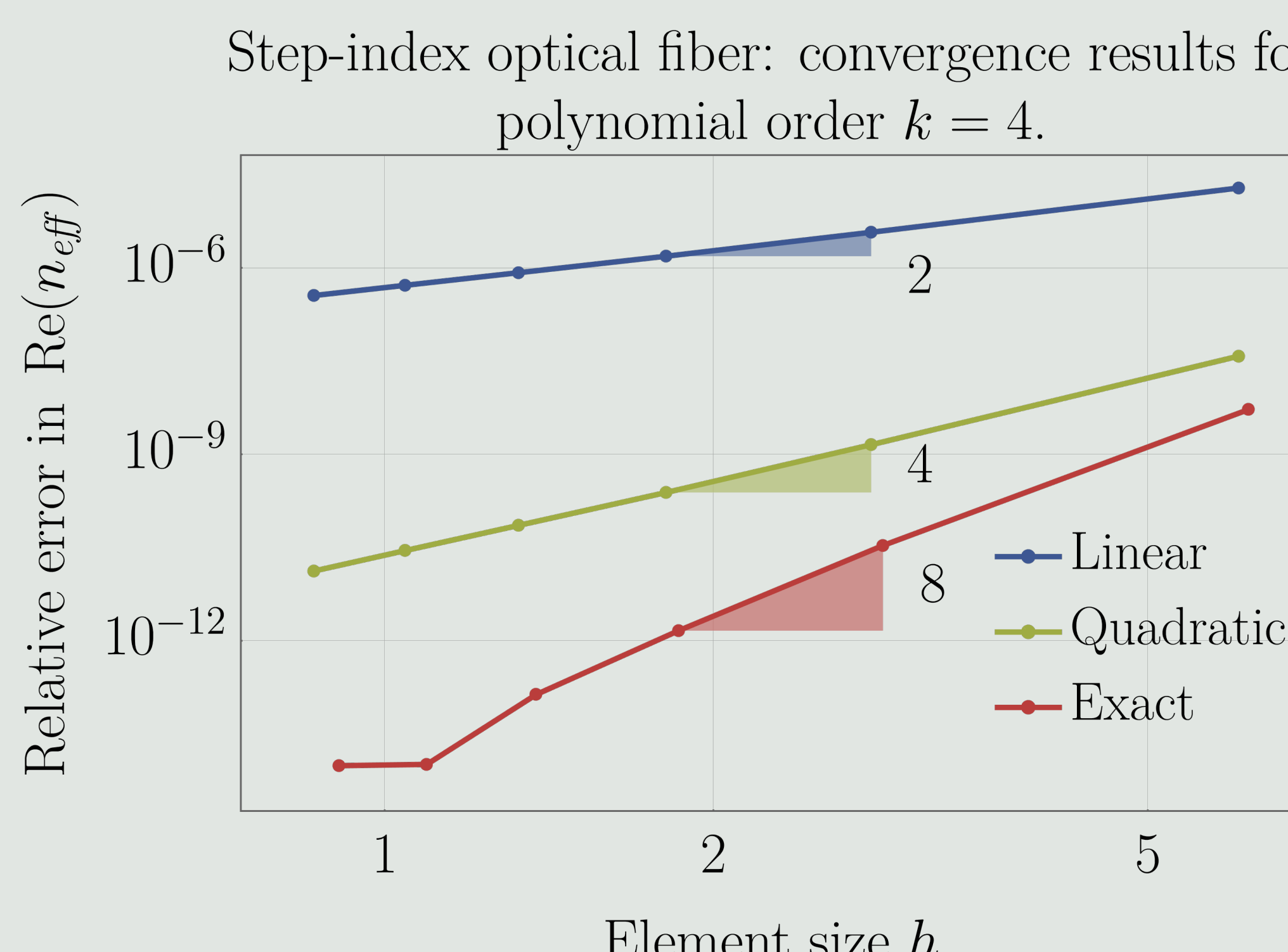


Figure 1: Comparison of convergence rates for the real part of the effective index of a step-index optical fiber. The polynomial order $k = 4$ was used in all three approximations. The geometry was described with elements obtained by linear mapping (blue curve), quadratic mapping (green curve) and exact mapping (red curve).

The optimal convergence rate is only obtained with the non-linear mapping: with a fixed number of elements, the linear mapping achieved an error of 10^{-6} , the quadratic mapping obtained 10^{-11} , and a relative error of 10^{-13} was obtained with the exact mapped elements. Figure 2 shows two linear polarized modes on the step-index optical fiber.

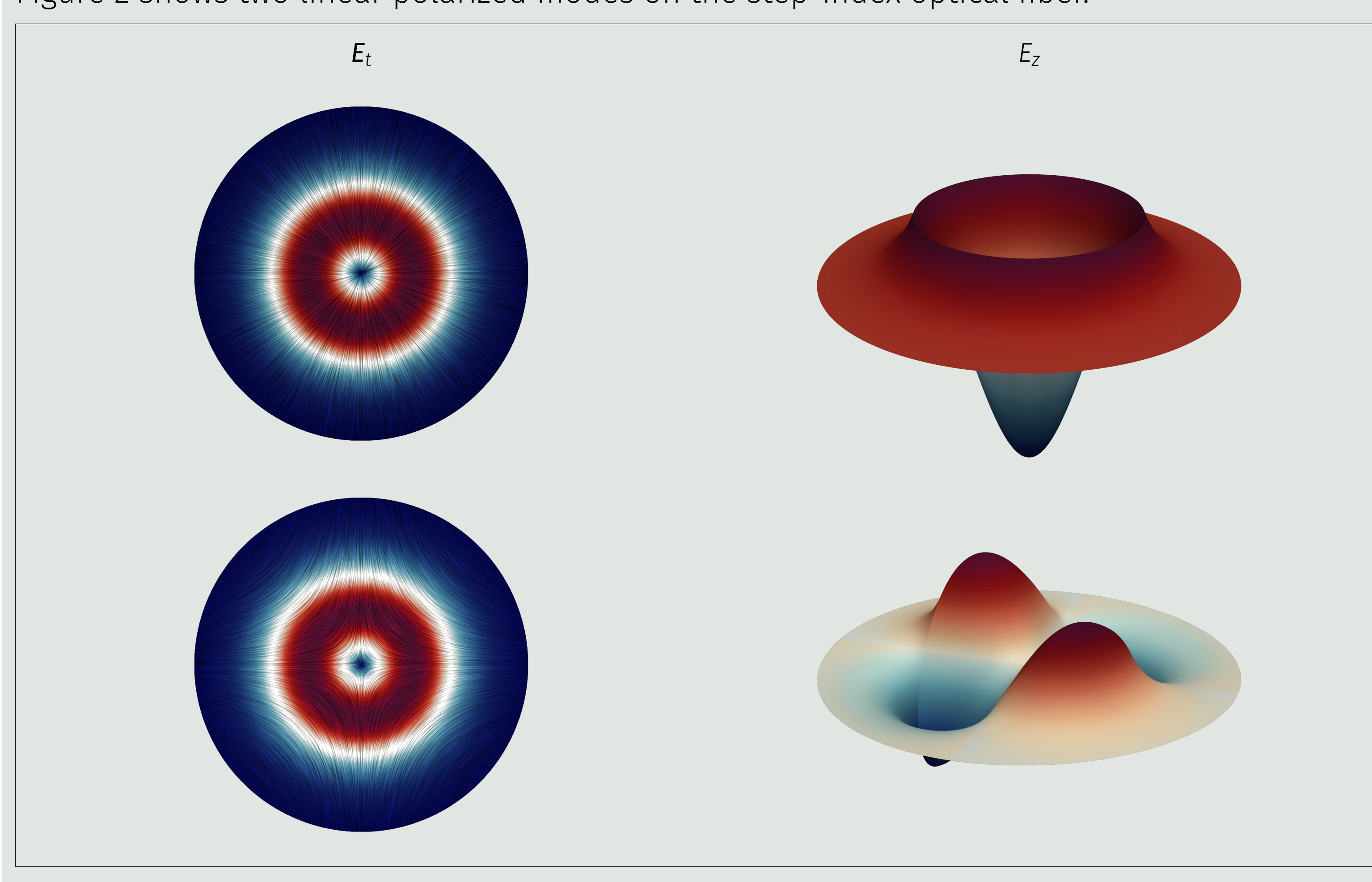


Figure 2: The first two approximated LP modes for a step-index optical fiber with $r_{\text{core}} = 8 \mu\text{m}$ and refractive indexes $n_1 = 1.4457$ (core) and $n_2 = 1.4378$ (cladding). The fiber is analyzed for $\lambda_0 = 1.55 \mu\text{m}$. On the left, the Line Integral Convolution of the transversal component of the electric field is shown, and on the right its correspondent longitudinal component.

4. HP-ADAPTIVITY CAPABILITIES

The developed basis functions, due to their hierarchical construction, can be easily integrated in the hp -algorithms of the NeoPZ framework[3]. In order to demonstrate its efficiency, the microstructured fiber presented in [4] was analyzed. Figure 3 shows a hp -adaptive mesh in which the refinements were performed upon observation of the solution obtained with a fine mesh.

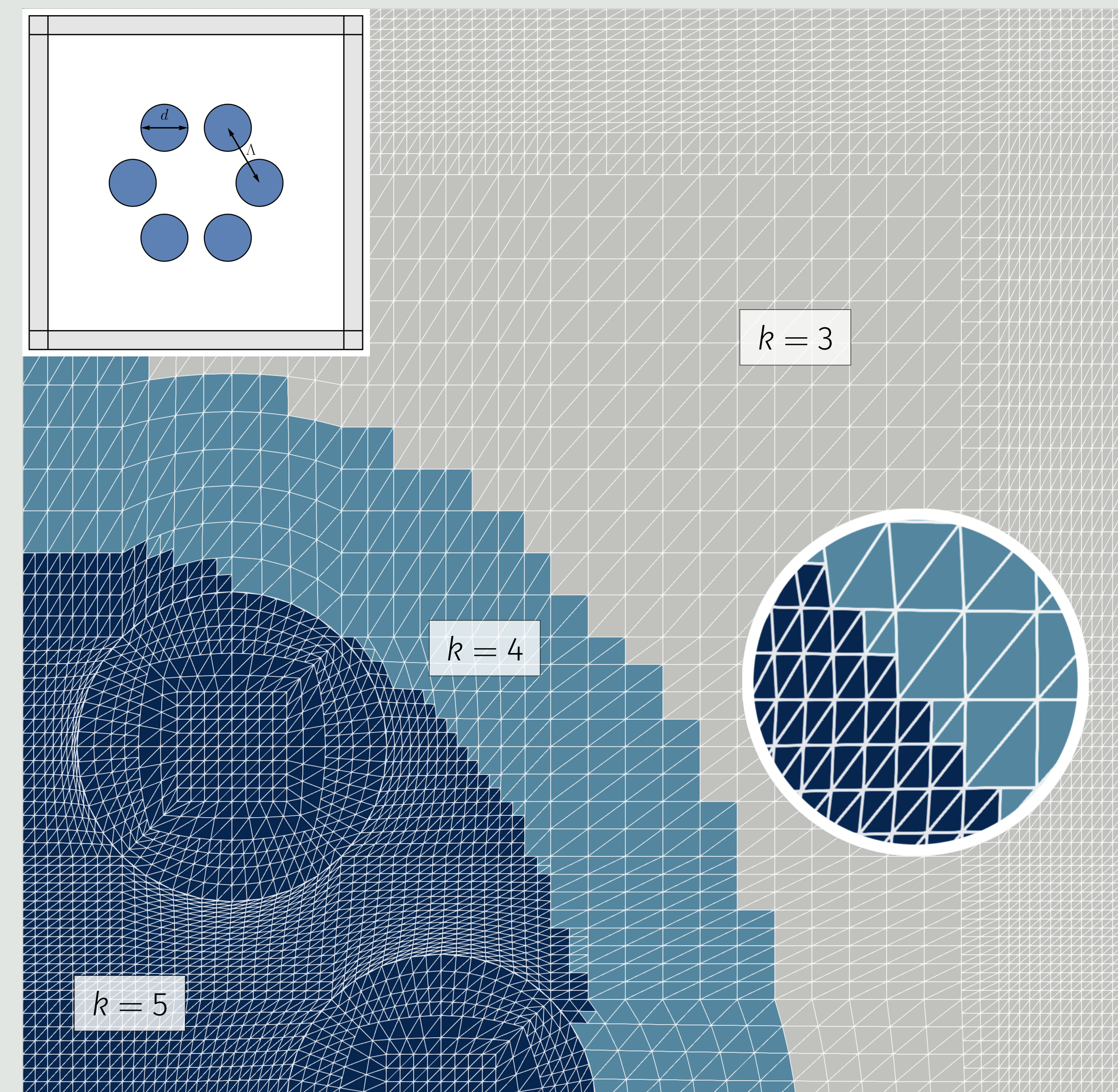


Figure 3: On the upper left, the cross-section(including the perfectly matched layers) of the microstructured fiber with six air-holes. The waveguide has a hole diameter of $d = 5 \mu\text{m}$ and a hole pitch of $\Lambda = 6.75 \mu\text{m}$. On the center, the FE mesh of the computational domain, which takes advantage of the symmetry of the desired fields, thus is a square with side $l = W + d_{\text{pml}}$, with $W = 15.75 \mu\text{m}$ and $d_{\text{pml}} = 2 \mu\text{m}$. The elements have varying polynomial order from $k = 3$ to $k = 5$, and the mesh was refined on the region near the holes. The detail on the right highlights the presence of hanging nodes in the mesh.

Table 1 shows the significant reduction on the number of equations when using p and hp -refinement. While the number of equations is still higher than the ones obtained with the pseudospectral method in Chiang and Chang [4], the sparsity of the FEM matrices, allied with a solver that supports Compressed Row Storage (CRS) as SLEPC[5] makes the FEM approach competitive in terms of memory and computational time. Finally, Figure 4 shows the electric field plots obtained with the mesh of Figure 3.

Table 1: Effect of hp mesh refinement on the number of equations and relative error of the approximated propagation constant in the microstructured fiber. In the example without refinement, $k = 5$ was used for all elements. On the other two simulations, $3 \leq k \leq 5$ was used, as shown in Figure 3.

mesh	n_{eq}	e_{rel}
—	285500	3.88420×10^{-13}
p	181992	3.38410×10^{-13}
hp	130476	9.86280×10^{-13}

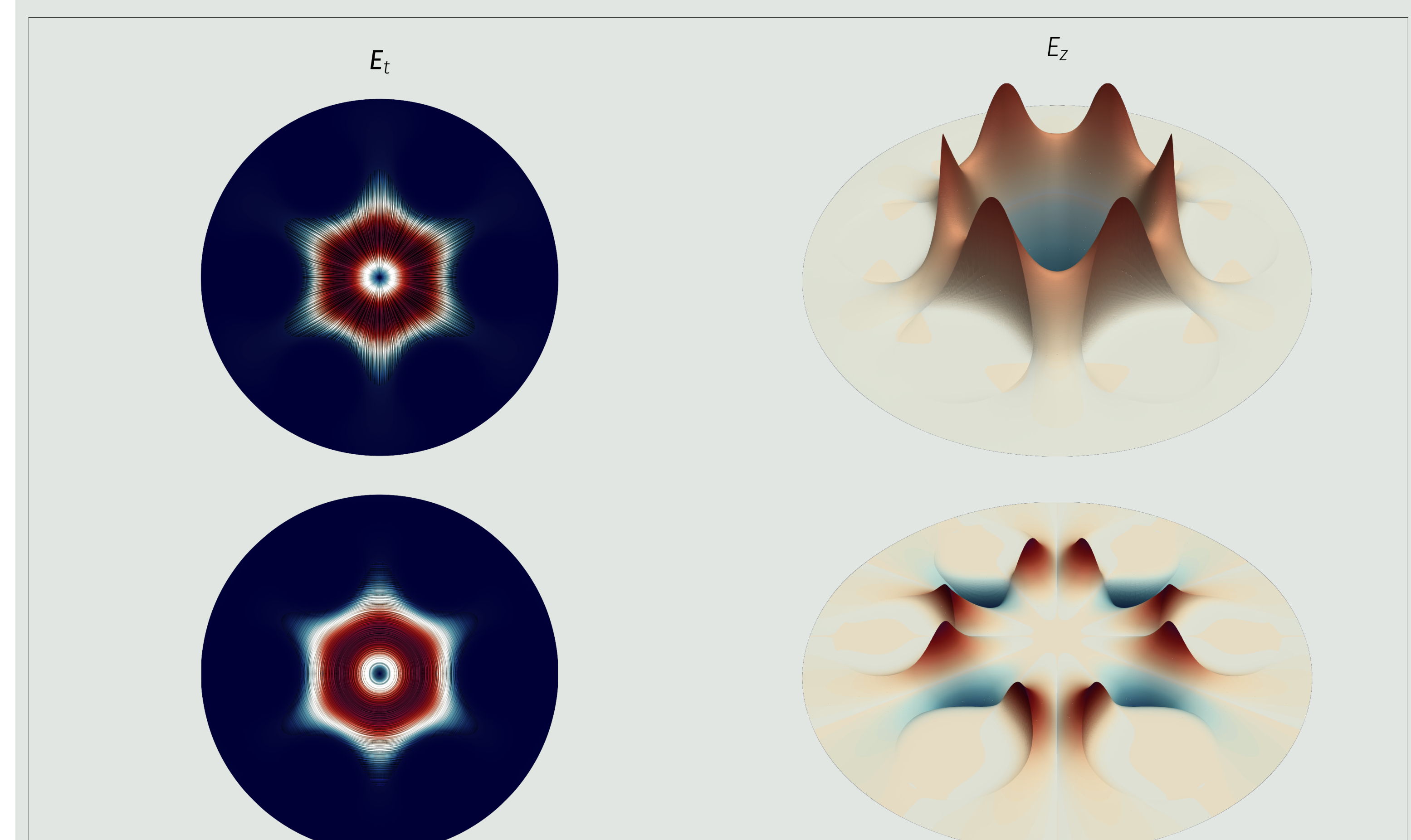


Figure 4: Electric field plot of the sixth (up) and third (down) non-degenerated electromagnetic modes of the microstructured fiber. On the left, the Line Integral Convolution of the transversal component of the electric field is shown, and on the right its correspondent longitudinal component.

REFERENCES

- [1] J.-M. Jin, *The Finite Element Method in Electromagnetics*. Wiley-IEEE Press, 2014.
- [2] J.-C. Nédélec, "Mixed finite elements in \mathbb{R}^3 ", *Numerische Mathematik*, vol. 35, no. 3, pp. 315–341, Sep. 1980.
- [3] J. L. D. Calle, P. R. Devloo, and S. M. Gomes, "Implementation of continuous hp-adaptive finite element spaces without limitations on hanging sides and distribution of approximation orders", *Computers & Mathematics with Applications*, vol. 70, no. 5, pp. 1051–1069, 2015.
- [4] P.-J. Chiang and H.-c. Chang, "A high-accuracy pseudospectral full-vectorial leaky optical waveguide mode solver with carefully implemented upml absorbing boundary conditions", *Opt. Express*, vol. 19, no. 2, pp. 1594–1608, Jan. 2011.
- [5] V. Hernandez, J. E. Roman, and V. Vidal, "SLEPC: A scalable and flexible toolkit for the solution of eigenvalue problems", *ACM Trans. Math. Software*, vol. 31, no. 3, pp. 351–362, 2005.